Experimental investigation and simulation of heat flux into metallic surfaces due to single discharges in micro-electrochemical arc machining (micro-ECAM)

Harry Krötz, Raoul Roth & Konrad Wegener

The International Journal of Advanced Manufacturing Technology

ISSN 0268-3768
Volume 68
Combined 5-8

Int J Adv Manuf Technol (2013)
68:1267-1275
DOI 10.1007/s00170-013-4918-9

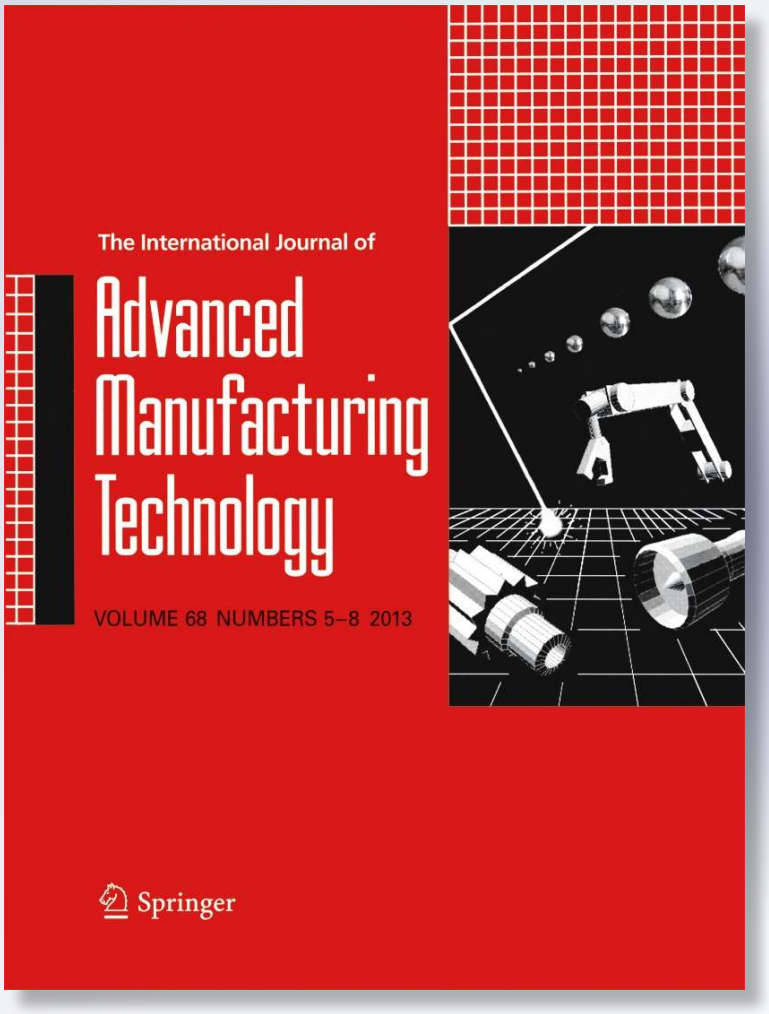

Springer

Int J Adv Manuf Technol (2013) 68:1267–1275
DOI 10.1007/s00170-013-4918-9

ORIGINAL ARTICLE

Experimental investigation and simulation of heat flux into metallic surfaces due to single discharges in micro-electrochemical arc machining (micro-ECAM)

Harry Krötz · Raoul Roth · Konrad Wegener

Received: 7 September 2012 / Accepted: 13 March 2013 / Published online: 24 April 2013

Abstract In this work, single discharges of electrochemical arc machining are examined. The heat-affected zone is analyzed, and a model is set up to simulate the heat transfer into the workpiece. As an input parameter of the simulation, the temperature of the electrochemical arc machining process was determined to be 3,500 K by means of emission spectroscopy. The simulation shows that the diameter of the heat-affected zone is less dependent on discharge duration and heat transfer due to heat flux than on the arc spot diameter. As a result of the investigation, it became clear that varying diameters of the heat-affected zone have to evolve from different diameters of the plasma channel's arc spot. Understanding the heat distribution into the workpiece in electrochemical arc machining with micro-machining parameters allows the further development of a micro-drilling process for electrically conductive materials based on electrochemical arc machining.

Keywords ECDM · ECAM · Micro-drilling · Single discharge · Heat flux · Simulation model

H. Krötz (✉) · R. Roth · K. Wegener
Institute of Machine Tools and Manufacturing, Tannenstrasse 3, 8092 Zürich, Switzerland
e-mail: harry.kroetz@gmx.de

R. Roth
e-mail: Raoul.Roth@iwf.ethz.ch

K. Wegener
e-mail: Konrad.Wegener@iwf.ethz.ch

Present Address:
H. Krötz
Eldec Schwenk Induction GmbH, Otto-Hahn-Strasse 14, 72280 Dornstetten, Germany

1 Introduction

Several manufacturing processes for drilling micro-holes into metallic materials are known. Electrochemical processes, such as electrochemical machining (ECM) are widely used in order to finish metallic surfaces. ECM is also used to finish micro-holes [1]. ECM needs a conductive medium, an electrolyte, to form an electrolyte cell including the workpiece conducted as anode and the tool electrode conducted as cathode. To drill and finish micro-holes with the same machining setup, power source, and working medium, manufacturing needs to take place within an electrolyte. If such a drilling process is developed, the mass flow calibration of a throttle plate for example can be done immediately after micro-drilling by electrochemical finishing. Using the electrochemical discharge phenomenon to machine hard and brittle materials is a technique in the field of non-conventional machining. Two manufacturing processes using this phenomenon and having the potential to drill holes and micro-holes are electrochemical discharge machining (ECDM) and electrochemical arc machining (ECAM).

In case of ECDM, the cathode which is normally made of copper acts as tool electrode. The anode is made of inert material. Both cathode and anode are immersed into an electrolyte. Thus, an electrolyte cell is formed similar to that of ECM. Applying a voltage to that electrolyte cell, hydrogen gas bubbles evolve on the cathode surface. They grow in size and restrict the current path between the cathode and electrolyte interface, causing discharges to occur at this interface instantly. The workpiece is not part of the electrolyte cell, but is immersed into the same electrolyte as the anode and cathode. The workpiece is either electrically conductive or non-conductive and is arranged in a short distance to the tool tip, where the discharges occur.

The material removal takes place by melting where the discharge strikes the surface of the workpiece [2]. The anode does not take part in the machining process and is termed non-machining electrode [3]. As conductive media, different types of electrolyte can be used. The power source can also differ depending on the machining process. To machine glass or various ceramics, [4] uses NaOH as an alkaline electrolyte and a DC voltage source. This variant of ECDM is termed spark-assisted chemical engraving. Pyrex glass is machined by [5] using KOH as alkaline electrolyte and a pulsed voltage source with pulse-on time of 2 ms. Soda lime glass and Al_2O_3 are machined with NaOH by [7] using a DC power supply. They termed the process electrochemical spark machining. HCl as acidic electrolyte and DC voltage is used in [2] to machine the electrically conductive materials silicon, brass, copper, and tantalum. The amplitude of the discharge current varies depending on the used material. The single discharge's affected zone was found to be round in nature with a diameter of 300 µm in case of a copper workpiece, a discharge current of about 16 A and a discharge time of approximately 1 ms. Metal removal formed an inner shining, round spot of about 60 µm in diameter.

With ECDM, electrically conductive or non-conductive materials can be machined. But ECDM micro-drilling is only used for non-conductive materials like Pyrex glass [6]. The fact that the workpiece is conducted neither as anode nor as cathode incapacitates ECDM as a micro-drilling process combined with electrochemical finishing.

The main difference between ECDM and ECAM is the arrangement of the anode and cathode. The non-machining electrode in ECDM which is conducted as anode is removed and the workpiece itself takes over this task. Thus, only electrically conductive materials can be machined. In ECDM, the discharges take place between the tool and the electrolyte, whereas the discharges take place between the tool and the workpiece in ECAM. ECAM is a modification of electrical discharge machining (EDM) where the dielectric medium of EDM is replaced by an electrolyte. EDM is well known to machine small and precise micro-holes with dimensions of about 100 µm in diameter. But if an electrolyte is used that leads to ECAM, there are no reports of machined micro-holes in literature.

There are several applications of ECAM in the field of machining metallic materials like smoothing surfaces, turning, wire cutting, and hole drilling [8]. The latter application is used for fine-hole drilling using a tubular tool with isolated side walls. Till now, micro-holes are not machined with ECAM.

The present work reveals the thermal effects of the arc spot of a plasma channel where the discharge strikes the surface of the workpiece, when ECAM is applied with micro-machining parameters like short pulse-on time and a small current value. Kojima et al. [9] showed that the arc plasma diameter in EDM is increasing with discharge time when using currents up to 17 A and discharge times up to 25 µs. Alike in case of ECAM [10] reported the increase of the arc plasma diameter with discharge time. It is said that short discharge duration is desirable for ECAM for better machining efficiency because a small plasma diameter at the end of the pulse-on time leads to an improved melt removal when the arc collapses. If this effect of arc channel widening affects the material removal mechanism in micro-ECAM is not yet clarified. Plasma channel formation time is reported to be 50 ns by [12].

In this work that is focused on micro-drilling, the used parameters have small values in order to achieve precise results and to protect the thin tool electrode having dimensions of about 100 µm in diameter of melting while drilling. The used current in this work is limited to 1 A. The pulse-on time is 1.5 µs while the pulse-off time is 2 µs.

2 Experiment

When a voltage is applied across the electrolyte cell, hydrogen gas evolves on the cathode surface and oxygen gas on the anode surface by means of electrolysis. The higher the applied voltage, the more gas is formed. Since the surface of the tool electrode is much smaller than that of the anodic workpiece, the tool electrode is covered by gas much faster than the workpiece. The resistance between the tool electrode surface and the electrolyte interface increases with the evolution of the gas layer. Electrochemical discharge starts only if the potential drop across this gas layer is higher than a critical value [3]. If the whole surface of the tool electrode is covered by gas and a sufficiently high voltage is applied, the gas becomes ionized due to the Townsend mechanism [13, 14].

In the mean stationary I-U characteristics, there are five different regions identified as summarized in [15]. After the thermodynamic region, there is an ohmic region describing ohmic behavior of the cell up to a limit voltage U_{lim}. Exceeding U_{lim}, the limiting current region follows with gas bubbles coalescing on the electrode surfaces and an increased bubble coverage fraction. This region ends when the critical voltage U_{crit} is reached. Further increase of the applied voltage up to the value 1.2 U_{crit} conveys through the transition region where a compact gas film arises around the tool electrode. With even higher voltages than 1.2 U_{crit}, the arc region starts where sparking occurs. The range of the limiting current region strongly depends on the electrolyte. For very concentrated electrolyte, the limiting current region vanishes while all other regions are still present [15]. The limiting current region is closely related to the formation of the gas film that covers the electrode surface. Certain mechanisms and parameter either lead to or influence the sudden

formation of the gas film. They include but are not limited to electrolyte concentration, changing wettability of the electrode, diameter of the electrode, hydrodynamic instabilities, or joule heating [14, 15].

An alkaline solution is typically used as electrolyte for the ECDM process, while an alkaline solution of Na_2SiO_3 as well as a saline solution of NaCl is reported in ECAM [10]. To keep the manufacturing system in the present work as simple as possible, no acidic or alkaline solution is used. This avoids complex and costly electrolyte conditioning and permits the use of machining equipment made of standard materials. Good results were achieved in own researches with a solution of sodium nitrate ($NaNO_3$). It is a typically used saline electrolyte in ECM and was also used in these experiments.

In literature, the operational voltage for ECDM using the alkaline electrolyte NaOH with 20–30 wt% is stated to be in the range of about 70–90 V when a 50-Hz sine-wave form of a pulsed DC power supply and a copper tool electrode with a diameter of 2 mm is used [11]. A pulsed voltage with an amplitude of 40 V and a pulse-on/-off time in the range of about 2 ms was applied in [5]. The used electrolyte was KOH with a concentration of 27.5 wt% and the tool electrode (200 µm in diameter) was made of wolfram carbide. In case of an acidic electrolyte (5 % HCL), an operational DC voltage of 155 V is reported in [2].

In this work, a solution of sodium nitrate with a conductivity of 25 mS/cm, which corresponds to a concentration of about 2.6 wt %, is used as electrolyte. The current of the energy source is pulsed in the range of 2 µs and limited to 1 A to protect the thin tool electrode having dimensions of about 100 µm in diameter from thermal damage. Using that parameter, the minimal voltage at which discharges occur was examined in own experiments for different electrolytes with the setup shown in Fig. 1.

The results are summarized in Table 1 and indicate the operational voltage that is needed to achieve coalescing gas bubbles in order to form a compact gas layer and to enter the arc region.

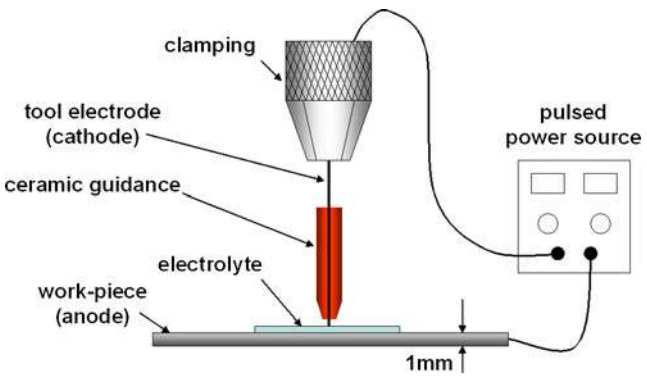

Fig. 1 Experimental setup of micro-drilling with ECAM

Table 1 1.2 U_{crit} [V] at 25 mS/cm

$LiNO_3$	NaCl	$NaNO_3$	KSO_4	$Zn_3(NO_3)_2$	HNO_3
40	45	55	60	90	110

As shown in Table 1, the voltage at which the first discharges strike through the compact gas film is 55 V in case of sodium nitrate. It is assumed that by applying a voltage of 85 V as done in further experiments, the permanent presence of a compact gas film is guaranteed. To confirm this assumption, the plasma formation at the cathode tool electrode was filmed with a high-speed camera and an arrangement of the electrodes as it is used in ECDM. The anode electrode and cathode tool electrode with a diameter of 100 µm are immersed into a solution of sodium nitrate having a conductivity of 30 mS/cm. They are arranged in a distance of 30 mm to each other. A pulsed voltage of about 85 V with a pulse-on time of 1.5 µs and a pulse-off time of 2 µs is applied to this electrolyte cell. Figure 2 shows subfigures that are taken with the high-speed camera MiniVis from Weinberger every 1.245 ms that corresponds to 803 fps. In the second picture, the whole electrode surface is covered with gas bubbles and the plasma formation takes place at first at the tool tip of the electrode. This is the point with the highest field strength and thus with the highest current density. It then moves upwards due to ohmic heating of the electrolyte causing generation of vapor bubbles that also take part in the formation of the gas layer.

In the high-speed camera experiment, the tool electrode was immersed into the electrolyte by about 6–7 mm. The current was limited to 1 A. In further experiments, where single discharges are examined, the tool electrode is immersed into the electrolyte for less than 1 mm like shown in Fig. 1. Consequently, the current density is much higher than in case of the high-speed camera experiment and so the compact gas film is assumed to be ensured for all further experiments. Figure 1 shows a schematic diagram of the experimental setup of micro-ECAM.

The tool electrode, which is made of tungsten with a diameter of 100 µm, operates as cathode and is centered by a ceramic guidance. The experiments are carried out without rotation of the tool electrode. The tip of the tool electrode is arranged in a small distance to the surface of the anodic workpiece. The surface of the workpiece is covered with a thin layer of electrolyte of about 150 µm in thickness. The electrolyte is a solution of $NaNO_3$ with a conductivity of 25 mS/cm. The workpiece is a plate of 1 mm thickness and is made of 100Cr6 steel. The decision to use 100Cr6 steel as workpiece material, that is a common material for gasoline injection systems, is attributed to the idea of mass flow calibration of a throttle plate after micro-drilling. Later on,

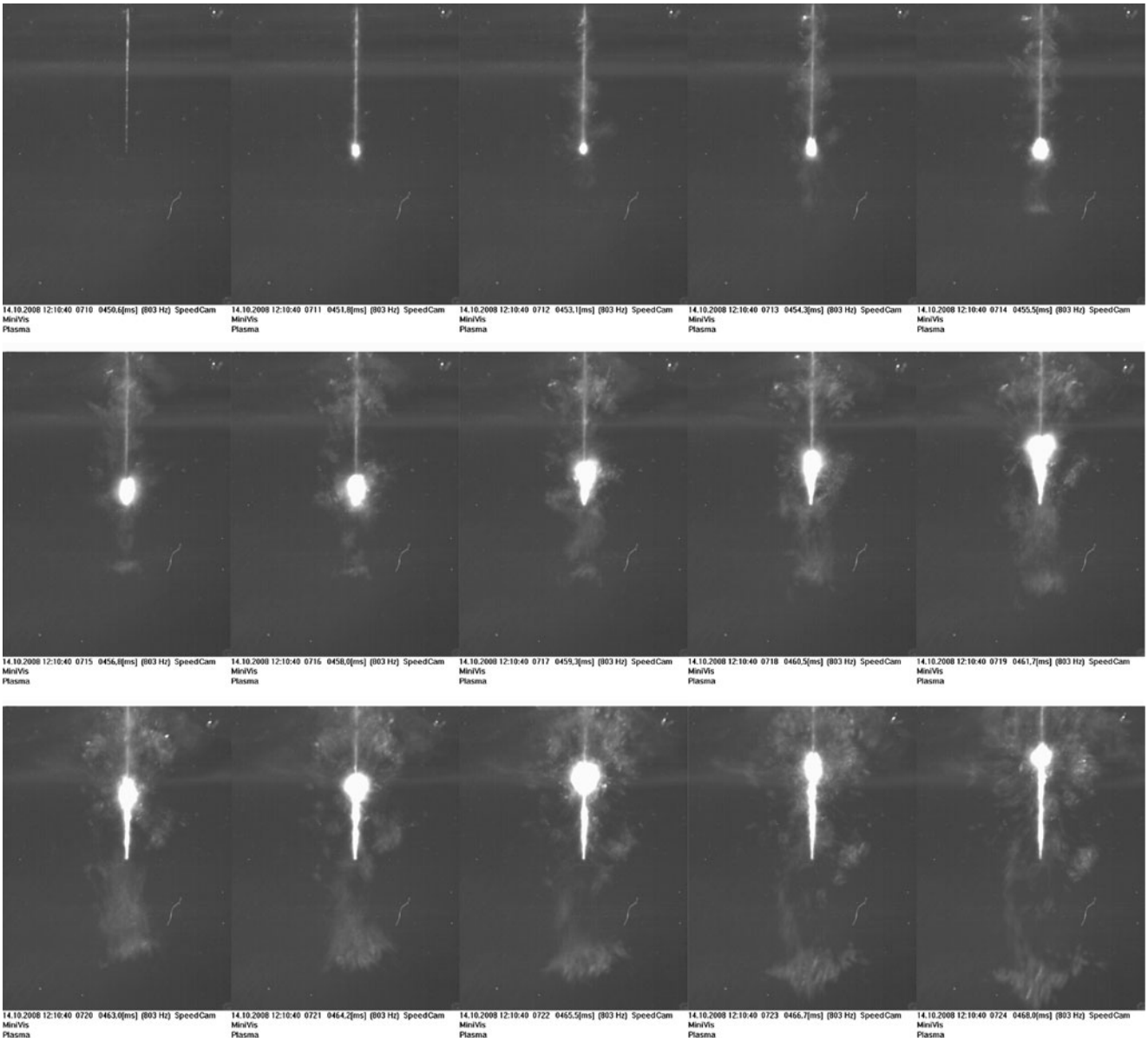

Fig. 2 Plasma formation at the cathode tool electrode with 100 µm in diameter immersed into an sodium nitrate electrolyte with a conductivity of about 30 mS/cm. The applied voltage is 85 V

X5 CrNi18-8 steel is used in one of the experiments, too. Just like 100Cr6, it is a common material for gasoline injection systems. To control the gap width, the average voltage between workpiece and tool is measured and compared to a threshold voltage to pull back or feed forward the tool electrode. During micro-ECAM, the applied voltage is provided by a programmable power source with an amplitude of 85 V. The maximum current is limited to 1 A. Pulse-on time is 1.5 µs, while the pulse-off time is 2 µs. The applied voltage amplitude was chosen based on the results in [16], where a solution of NaCl and $NaNO_3$ was used to study the discharge mechanisms in ECAM. The oscilloscope graphs are recorded by the Tektronix oscilloscope TDS2000C, and the current is directly measured on the clamping mechanism with the Tektronix AC/DC current probe TCP0030.

The experiments are carried out in three different experimental setup variants.

1. The ceramic guidance is present, and the gap between the tool electrode and workpiece is kept constant at 4 µm.
2. The ceramic guidance is removed to permit lateral movements of the electrode, and the distance to the workpiece is controlled by the gap control of the experimental setup.

3. The ceramic guidance is present, and the gap between the tool electrode and workpiece is controlled by the gap control.

In the first and second variants, single discharges are applied and the heat-affected zone (HAZ) is analyzed. Different diameters of the HAZ are found on the surface of the workpiece. In the third variant, a micro-blind hole is drilled.

2.1 Setup variant 1

Twenty voltage pulses are applied across the electrodes. Total machining time is 70 µs. Figure 3 shows the resulting voltage and current curves measured with a digital storage oscilloscope. Channel 3 shows the applied voltage and channel 1, the resulting current. The first 18 pulses are needed to create the necessary gas layer on the cathodic surface. Any material removal so far takes place electrochemically. Afterwards, two discharges occur subsequently, identifiable on the high peaks in the oscillograph curves. While discharges take place, the voltage across the electrode gap breaks down to the arc voltage of about 10 V. The current is the maximum current of 1 A. The high peaks, which are visible in both channels during breakdown, are not representing a physical increase in current or voltage but are disturbances that couple into the wires of the measuring equipment. By changing the position of the wires, the peaks are reversed. The source of the disturbance is the high voltage derivative with respect to time dV/dt occurring during breakdown. Since the peaks are defining precisely the breakdown moment (when the voltage in channel 3 breaks down to the arc voltage), no effort is made to dampen or filter them out.

Figure 4 shows the HAZ. As no other arc spot is found, it might be that the diameter results from the arc spot of both discharges that stroke the workpiece at the same location. The HAZ is larger than the melting zone. The diameter within which melting occurs is about 20 µm. It is obvious

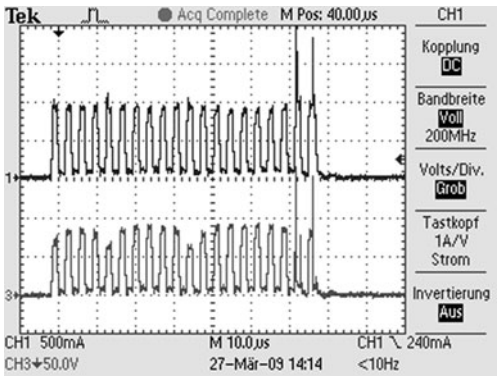

Fig. 3 Oscillograph curves of voltage and resulting current of 20 ECAM pulses in sodium nitrate

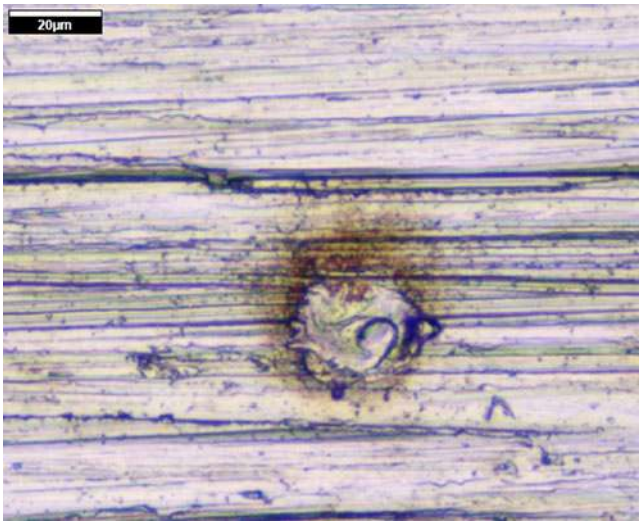

Fig. 4 Heat-affected zone of one single or two consecutive discharges, pulse duration 1.5 µs

that the material in this area was molten but not removed from the bulk material. The molten material resolidified on the surface of the workpiece.

2.2 Setup variant 2

The ceramic guidance is removed to permit lateral movements of the electrode. The gap width is not constant, but controlled by the gap control. The tool electrode is moved forward or backward, depending on the average voltage measured between the anode and cathode. Voltage pulses are applied with the same duration and amplitude like in setup variant 1 for about 17 s that corresponds to 4,857,142 voltage pulses. The melting zones of the latest arc spots are

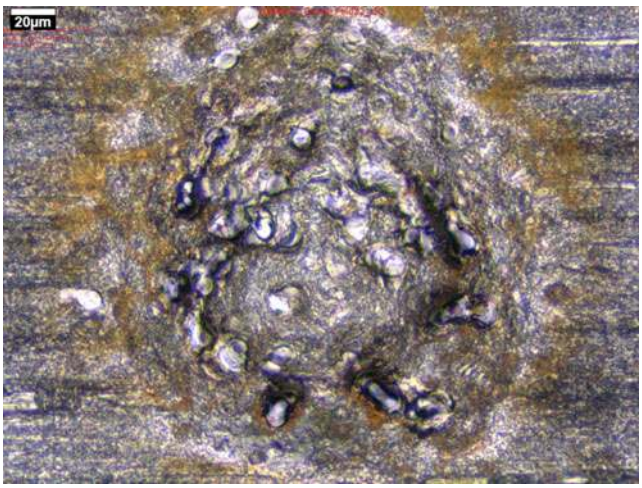

Fig. 5 Arc spots on the surface with permanent pulsing and unguided electrode, machining time was 17 s

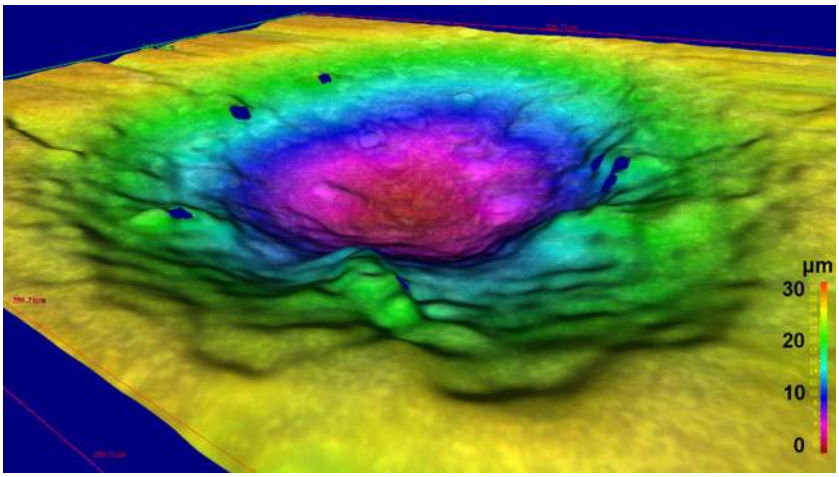

Fig. 6 Topography of the machined surface shown in Fig. 5

still visible. Those that occurred earlier are electrochemically finished and less clear to see (Fig. 5). Since the tool electrode is not guided in this experiment, the machined surface is widely spread and a drilling depth of only 30 µm is achieved. Figure 6 shows the topography of the machined surface. The diameters of the arc spots are within the range of 8–12 µm.

2.3 Setup variant 3

To identify the depth of molten material in the HAZ, a blind hole of 500 µm in depth is machined with the same tool electrode and the same drilling parameters like in setup variants 1 and 2. The tungsten tool electrode is guided by the ceramic guidance, machining time is 33 s. The workpiece material is X5 CrNi18-8 steel. Figure 7 shows the resulting shape of the machined blind hole.

Only the ground of the blind hole is examined. Since the temperature in this area is very high while drilling, no liquid electrolyte is present and no electrochemical machining is possible to influence the surface and reduce the layer thickness. The white layer on the hole wall, which represents the molten and resolidified material, has a thickness of about 3 µm. The annealing area is about 1 µm thick (Fig. 8). Since the latest visible arc spots in Fig. 5 are spread over the whole machined surface, it is assumed that they are also spread over the whole machined surface in this experiment. Thus, the thickness of the white layer represents the order of magnitude of depth in which melting occurs while ECAM micro-drilling.

3 Modeling

In the Figs. 4, 5, and 8 the heat-affected zone of single discharges and a drilled micro-blind hole are shown. The diameter of a single discharge is in the range of about

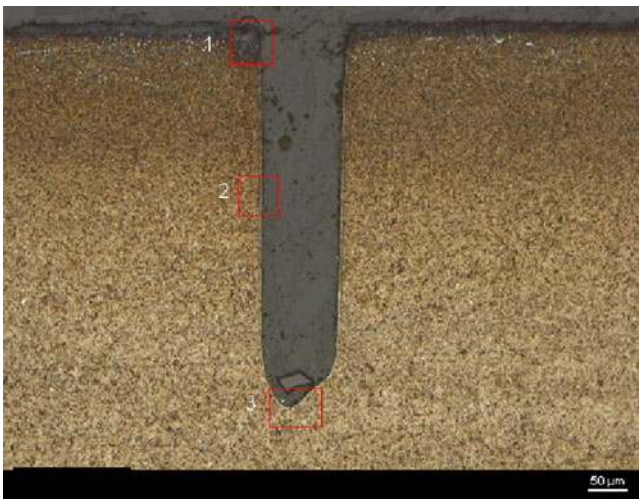

Fig. 7 Shape of a blind hole machined with micro-ECAM

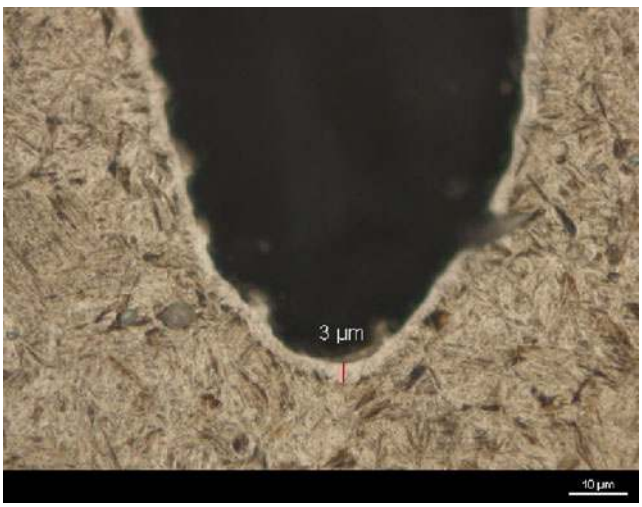

Fig. 8 Heat-affected zone of a blind hole machined with micro-ECAM

8–20 µm. The depth of the recast layer is up to 3 µm. To see the nature of heat flux under micro-ECAM conditions and to understand the influence of the plasma arc spot as a heat source, a model is set up to simulate the heat transfer during discharge.

In EDM, the plasma temperature is reported by [17] to be 6,000–7,000 K, using a discharge current of 40 A and a discharge time of 300 µs. In case of EDM, [12] has shown that the plasma develops very fast (<50 ns) and subsequently remains quite stable during the rest of the discharge. The used voltage was 200 V and the discharge current was 8 A.

In this work, using micro-drilling parameters, the discharge current is 1 A and the discharge time is 1.5 µs. The plasma temperature under these conditions is determined in own researches by means of emission spectroscopy. The OH radical in a plasma is in a thermal equilibrium with its surrounding area. Due to interpretation of the light emitted by the OH radicals when changing their rotatory orientation, the ECAM plasma temperature is determined to be 3,500 K. It is assumed that the plasma formation in ECAM takes place within the same time range like in EDM. This means that the plasma formation time is much smaller than the discharge time of 1.5 µs in the previous experiments. For this reason, the growth of the plasma channel is neglected in this model.

To simulate heat transfer into the bulk material, the model is set up with dimensions as shown in Fig. 9. Considering the machined surface, shown in Fig. 5, the heat source of the model that represents the arc spot of the plasma channel is assumed to be a disk-shaped area with a diameter of 10 µm. Using COMSOL Multiphysics, the model is implemented as a two-dimensional, cylinder symmetrical model. This means that the heat source is implemented as a linear line with a length of 5 µm. Initial and boundary conditions are as follows:

- left boundary: symmetry axis, no heat flux possible
- heat source on the top: predefined temperature, 3,500 K
- all other boundaries: thermal isolation, as the cooling on the surface is much slower than the heating in the plasma arc spot
- At time $t = 0$, the whole body is at 292 K

Equation 1 shows the general equation that describes heat transfer due to heat flux and convection within a liquid at constant pressure.

$$\rho C_p \frac{\delta T}{\delta t} + \nabla \cdot (-k \nabla T) = Q - \rho C_p u \cdot \nabla T \tag{1}$$

The purpose of this model is to simulate heat transfer into a solid workpiece by conduction. So the right side, right term that takes into account convection, is reduced. The result is Eq. 2 that is used in the model to calculate the temperature distribution over the time.

$$\rho C_p \frac{\delta T}{\delta t} + \nabla \cdot (-k \nabla T) = Q \tag{2}$$

The equation describes the interplay between heat storage (left side, left term), heat flux (left side, right term) and intrinsic heat sources (right side). Where ρ is the density (in kilogram per cubic meter) and C_p is the specific heat capacity of the material at constant pressure (in joule per kilogram Kelvin). T stands for the absolute temperature (in Kelvin), Q is the volumetric power of a bulk heat source (in watt per cubic meter) which is assumed to be zero in this model, and k is the thermal conductivity (in watt per meter Kelvin) with isotropic nature in this model.

As latent heat, a value of 248 kJ/kg is used [18]. This value is consumed by the workpiece while melting. To get a smaller temperature gradient and, hence, smaller rounding errors while using coarse time steps, the latent heat is

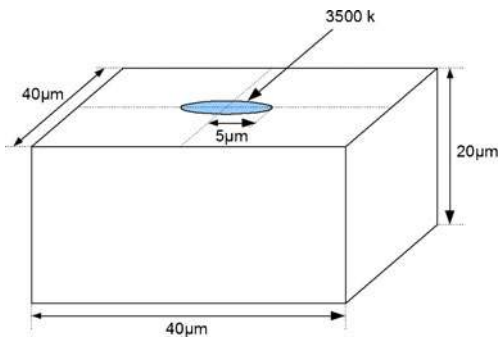

Fig. 9 Geometry of the simulation model

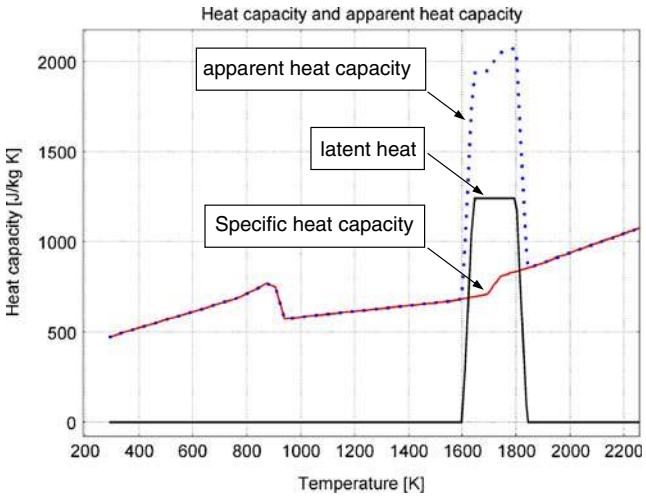

Fig. 10 Specific and apparent heat capacity used in the simulation

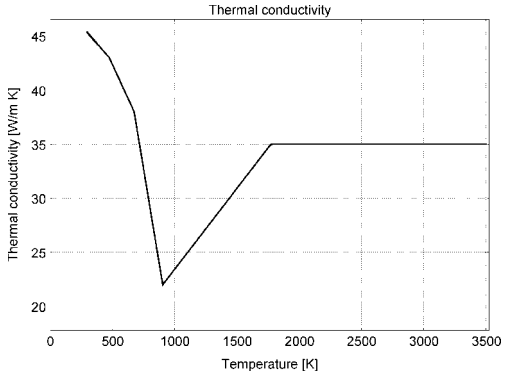

Fig. 11 Thermal conductivity k as a function of temperature

not consumed at once in this model, but over a temperature range of about 250 K.

The used apparent heat capacity, which is the sum of specific heat capacity and latent heat, is shown in Fig. 10 as a dotted line. The considered thermal conductivity is shown in Fig. 11. Both thermal conductivity and specific heat capacity are taken from [19] for steel with 0.6 % of carbon.

The simulation time was set to 2 µs. In the experimental study, the discharge duration in case of no ignition delay was 1.5 µs. The partial differential equation is solved numerically by COMSOL Multiyphysics with the finite element method. Figure 12 shows the temperature distribution after 1.5 µs.

The plotted continuous line that intersects the Y-axis at a depth of about 2.9 µm marks the isothermal of 1,720 K. This is the melting temperature of 100Cr6 steel. The diameter of the melting zone at the surface of the workpiece is 12 µm.

Looking at the solution at different instants of time in Figs. 13 and 14 reveals that when increasing the discharge

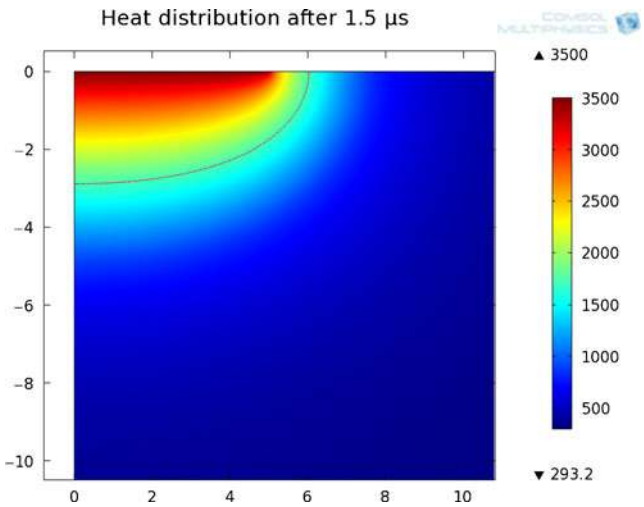

Fig. 12 Solution of Eq. 2 after 1.5 µs

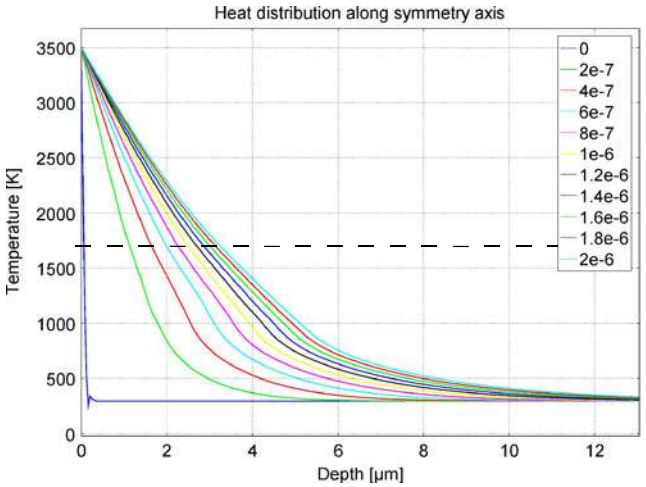

Fig. 13 Temperature distribution into the bulk material along the symmetry axis of the arc spot at different instants of time within a time range from 0.2 to 2 µs. The *dotted line* represents the isothermal of 1,720 K that is the melting temperature of 100Cr6 steel

time by 33 % from 1.5 to 2 µs, the isothermal of 1,720 K (dotted line) grows 10 % in depth and only 3.3 % in diameter. After 2 µs, a depth of about 3.2 µm is reached and a diameter of about 12.4 µm.

3.1 Results and discussions

Material removal in micro-ECAM does not take place due to melting and ejecting the melt like in normal ECAM or EDM. No small craters are formed like in EDM, where the plasma temperature is reported to be about 7,000 K. In micro-ECAM, the plasma temperature is 3,500 K. Material

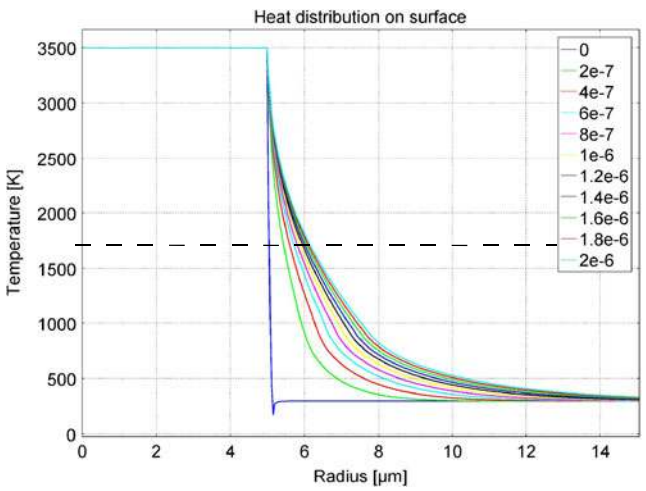

Fig. 14 Temperature distribution on the surface of the workpiece in the HAZ at different instants of time within a time range from 0.2 to 2 µs. The *dotted line* represents the isothermal of 1,720 K that is the melting temperature of 100Cr6 steel

removal takes place due to plasma etching and polishing the material that is located in the arc spot of the plasma channel. Figures 4 and 5 show that unlike in ECAM with high current values, no ejection of the melt takes place in micro-ECAM when the plasma channel collapses. Instead, the melt resolidifies on the surface. The depth of the recast layer of about 3 µm in Fig. 8 corresponds with the results of the simulation where a depth of about 2.9 µm is calculated, neglecting the ignition delay time.

The diameter of the melting zone equals to the diameter of the arc spot that is in the range of about 10 µm. Due to heat flux, the diameter is not increasing more than 2 µm within 1.5 µs considering Figs. 12 and 14. The melting zone in Fig. 4 with a diameter of about 20 µm cannot be explained by heat transfer, even if two consecutive discharges would have been occurred at the same place.

4 Conclusions

Considering the results of the simulation, the different diameter of the HAZ cannot be explained by heat transfer. On the other side, the simulation has shown that the diameter of the melting zone is almost equal to the diameter of the arc spot. Thus, a different melting zone diameter is the result of a different arc spot diameter.

Bigger diameters of the melting zone in the range of about 20 µm are only observed in setup variant 1 where single discharges are examined. In this constellation the composition and temperature of the dielectric medium that separates the anode and cathode from each other differs from the dielectric medium with permanent pulsing.

In case of just a few voltage pulses and, consequently, just a few discharges, the composition of the gas that separates anode and cathode when ignition takes place is a mixture of oxygen and hydrogen gas, formed at the electrode surfaces by electrolysis. The gas temperature is in the range of the electrolyte temperature.

In case of permanent pulsing, the temperature is highly increased and causes the electrolyte to evaporate. This leads to less oxygen and hydrogen formation but more vapor, ionized tool material and salt in the dielectric medium that separates anode and cathode from each other. These different conditions at the time of ignition influence formation and growth of the plasma channel that leads to different arc spots which, in terms, results in different diameters of the melting zone.

Small differences of the melting zone diameter of about 2 µm might be based on different ignition delay times and thus different discharge times.

References

1. Hung JC, Yan BH, Liu HS, Chow HM (2006) Micro-hole machining using micro-EDM combined with electropolishing. J Micromech Microeng 16:1480–1486
2. Kulkarni A, Sharan R, Lal GK (2002) An experimental study of discharge mechanism in electrochemical discharge machining. Int J Mach Tools Manuf 42(10):1121–1127
3. Ghosh A (1997) Electrochemical discharge machining: principle and possibilities. SADHANA 22(3):435–447
4. Wüthrich R, Hof LA, Lal A, Fujisaki K, Bleuler H, Mandin Ph, Picard G (2005) Physical principles and miniaturization of spark assisted chemical engraving (SACE). J Micromech Microeng 15:268–275
5. Zheng ZP, Cheng WH, Huang FY, Yan BH (2007) 3D microstructuring of Pyrex glass using the electrochemical discharge machining process. J Micromech Micromach 17(5):960–966
6. Zheng ZP, Su HC, Huang FY, Yan BH (2007) The tool geometrical shape and pulse-off time of pulse voltage effects in a Pyrex glass electrochemical discharge microdrilling process. J Micromech Micromach 17(2):265–272
7. Bhondwe KL, Yadava V, Kathiresan G (2006) Finite element prediction of material removal rate due to electro-chemical spark machining. Int J Mach Tools Manuf 46:1699–1706
8. McGeough JA, Rasmussen H (1990) A theoretical analysis of electrochemical are machining. Proc R Soc Lond A A429:429–447
9. Kojima A, Natsu W, Kunieda M (2008) Spectroscopic measurement of arc plasma diameter in EDM. CIRP Ann Manuf Technol 57:203–207
10. Crichton IM, McGeough JA, Munro W, White C (1981) Comparative studies of ecm, edm and ecam. Precis Eng 3(3):155–160
11. Bhattacharyya B, Doloi BN, Sorkhel S K (1999) Experimental investigations into electrochemical discharge machining (ECDM) of non-conductive ceramic materials. J Mater Process Technol 95:145–154
12. Descoeudres A, Hollenstein Ch, Wälder G, Perez R (2005) Time-resolved imaging and spatially resolved spectroscopy of electrical discharge machining plasma. J Phys D: Appl Phys 38(22):4066–4073
13. De Silva AK (1988) Process developments in electrochemical arc machining. PhD thesis, University of Edinburgh
14. Basak I, Ghosh A (1996) Mechanism of spark generation during electrochemical discharge machining: a theoretical model and experimental verification. Mater Process Technol 62:46–53
15. Wüthrich R, Comninellis Ch, Bleuler H (2005) Bubble evolution on vertical electrodes under extreme current densities. Electrochim Acta 50:5242–5246
16. Crichton IM, McGeough JA (1984) Studies of the discharge mechanisms in electrochemical arc machining. J Appl Electrochem 15:113–119
17. Kunieda M, Lauwers B, Rajurkar KP, Schumacher BM (2005) Advancing EDM through fundamental insight into the process. CIRP Ann 54/2:64–87
18. Wang W (2006) Simulation des Erstarrungsprozesses und des Inline-Walzens von im Strang gegossenen Stahlknüppeln mit flüssigem Kern. PhD thesis, Rheinisch -Westfälische Technische Hochschule Aachen
19. Jyrki M, Seppo L (1994) Calculation of thermophysical properties of carbon and low alloyed steels for medeling of solidification processes. Metall Mater Trans B 25B:909–916